AD-A111 451 NAVAL RESEARCH LAB WASHINGTON DC F/G 20/7
HEAVY ION FRAGMENTATION AT INTERMEDIATE ENERGY.(U)
MAR 82 J KIDD, N SEEMAN, S WOODS
UNCLASSIFIED NRL-MR-4733 NL

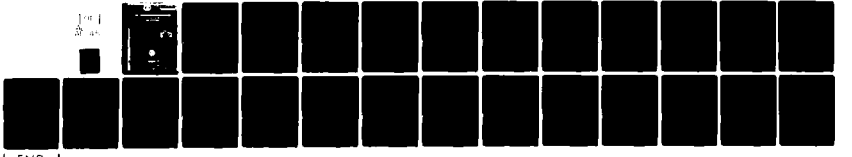

END
DATE FILMED
4-82
DTIC

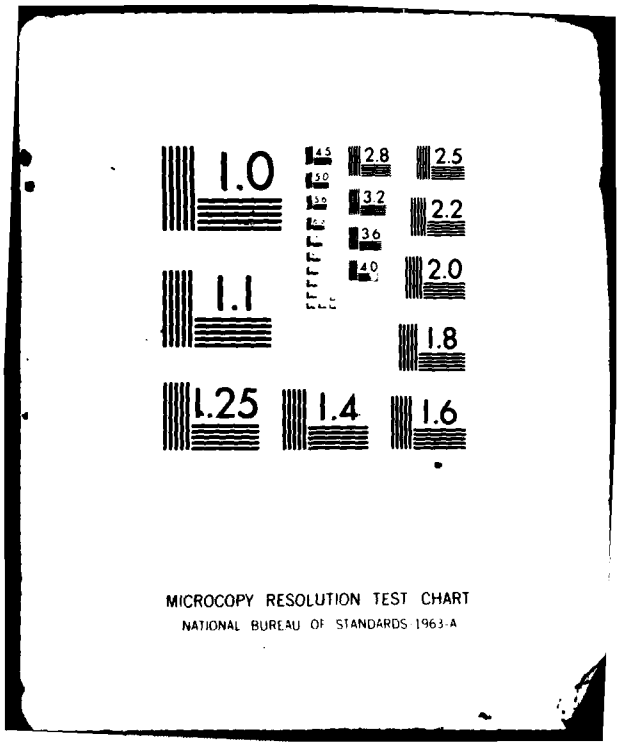
1.0
1.1
1.25
1.4
1.6
1.8
2.0
2.2
2.5
2.8
3.2
3.6
4.0
4.5
5.0
MICROCOPY RESOLUTION TEST CHART
NATIONAL BUREAU OF STANDARDS 1963-A

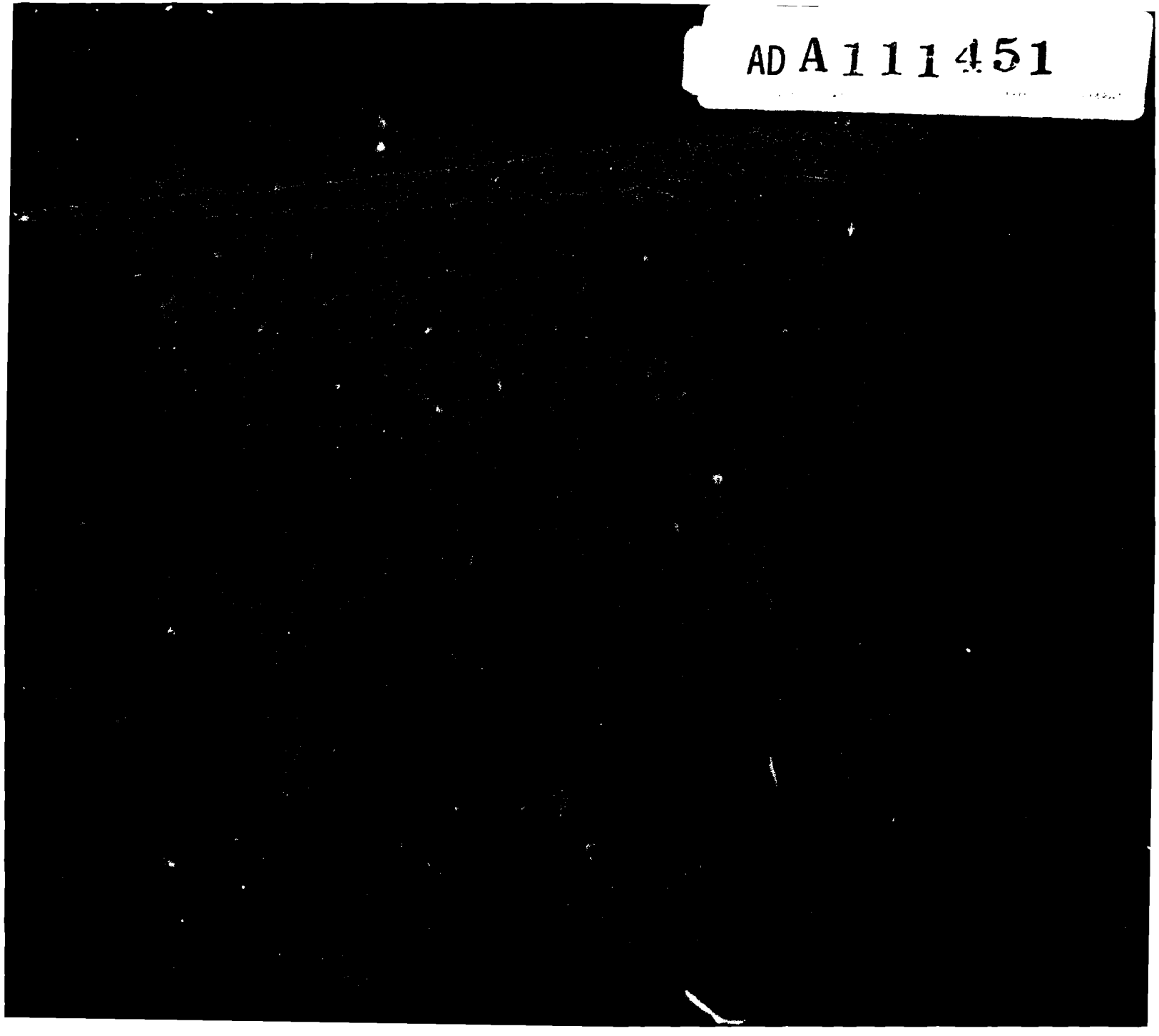

SECURITY CLASSIFICATION OF THIS PAGE (When Data Entered)

REPORT DOCUMENTATION PAGE		READ INSTRUCTIONS BEFORE COMPLETING FORM
1. REPORT NUMBER NRL Memorandum Report 4733	2. GOVT ACCESSION NO. AD-A113 451	3. RECIPIENT'S CATALOG NUMBER
4. TITLE (and Subtitle) HEAVY ION FRAGMENTATION AT INTERMEDIATE ENERGY		5. TYPE OF REPORT & PERIOD COVERED Interim report on a continuing NRL problem. 6. PERFORMING ORG. REPORT NUMBER
7. AUTHOR(s) J. Kidd, N. Seeman, and G. Woods		8. CONTRACT OR GRANT NUMBER(s)
9. PERFORMING ORGANIZATION NAME AND ADDRESS Naval Research Laboratory Washington, DC 20375		10. PROGRAM ELEMENT, PROJECT, TASK AREA & WORK UNIT NUMBERS 61153N; RR012-02-41; 66-0443-02
11. CONTROLLING OFFICE NAME AND ADDRESS		12. REPORT DATE March 1, 1982 13. NUMBER OF PAGES 25
14. MONITORING AGENCY NAME & ADDRESS(if different from Controlling Office)		15. SECURITY CLASS. (of this report) UNCLASSIFIED 15a. DECLASSIFICATION/DOWNGRADING SCHEDULE

16. DISTRIBUTION STATEMENT (of this Report)

Approved for public release; distribution unlimited.

17. DISTRIBUTION STATEMENT (of the abstract entered in Block 20, if different from Report)

18. SUPPLEMENTARY NOTES

19. KEY WORDS (Continue on reverse side if necessary and identify by block number)

Heavy ion fragmentation
Isotopic production cross sections
Isotopic momentum distributions
Heavy ion detection
Bevatron accelerator

20. ABSTRACT (Continue on reverse side if necessary and identify by block number)

The N.R.L. Heavy Ion Experiment, which was run at the Lawrence Berkeley Laboratory Bevatron Accelerator, measured the single-particle inclusive production cross sections and momentum distributions for carbon ions at 250 MeV/u incident on CU, C, CH_2 (and hydrogen) targets. The discussion of this experiment will include: 1) the detector design, 2) the beam monitoring system and fast logic, 3) the running system software and 4) the analysis and preliminary results.

The mass resolution achieved was $\Delta A/A \sim 0.15$ and the spatial resolution with the drift chamber was ~0.5mm. A separate report will discuss the final results and their implications.

DD FORM 1 JAN 73 1473 EDITION OF 1 NOV 65 IS OBSOLETE
S/N 0102-014-6601

SECURITY CLASSIFICATION OF THIS PAGE (When Data Entered)

CONTENTS

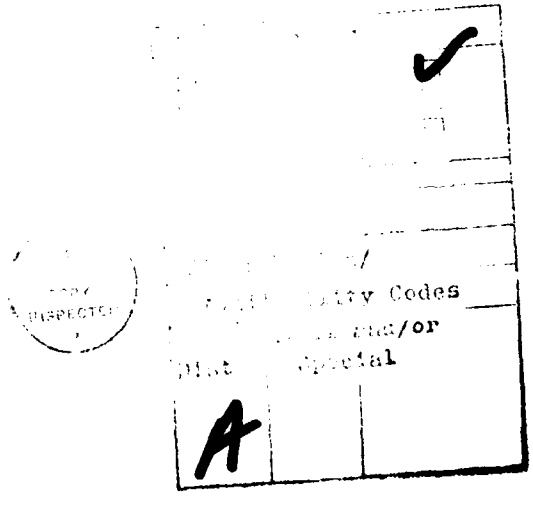

HEAVY ION FRAGMENTATION AT INTERMEDIATE ENERGY

1. Introduction:

The N.R.L. Heavy Ion Experiment was designed to study the single-particle inclusive reaction of ^{12}C ions at 250 MeV/u; that is, ^{12}C +Target→X + anything, where X is any final state fragment, within the small acceptance solid angle of the detector. The targets were Cu, C, and CH_2. Hydrogen data are obtained by double subtraction of C and CH_2.

The experiment measured:

A. Production cross sections for the 20 final-state isotopes at eight production angles for each target,

B. Momentum distributions (*longitudinal and transverse*) and widths for all isotopes for each angle and target .

The measurements were definitive and of high statistical accuracy. The entire data set with scaler data was 1.1×10^8 words of information.

Apart from their fundamental interest (this is the energy region in which one expects that the cross sections will be energy dependent), the results will be useful in a number of fields. Indeed, the preliminary results are already in use. Immediate applications will be:

A. Satellite vulnerability (transport calculations through satellite material, - soft upset modelling - N.R.L.)

B. Space shuttle (angular distributions, cross sections, effects on astronauts - N.A.S.A.)

Manuscript submitted December 7, 1981.

C. Bio-med (angular distributions and cross sections for treatment of cancer in humans with 250 MeV/u carbon ion beams - L.B.L.)

D. High Energy Astrophysics (propagation calculations in atmosphere and inter-stellar space, nucleus-nucleus semi-empirical relations - N.R.L.)

E. Nuclear structure (energy dependence of cross sections, factorization, limiting fragmentation, behavior of momentum distributions - N.R.L., L.B.L.)

F. Pellet fusion (energy dependence of reaction mechanisms - D.O.E.)

2. Detector Design Considerations:

The experimental layout is shown in Figure 1 and the detector is shown in Figure 2. Table I lists the detector components and materials. There were seven main signals from the detector for each event (a complete event was 34 words). The drift chamber measured the production angle and the S1 counter measured the charge. The signals produced by the Cherenkov and the two CsI counters were used to determine the velocity of the fragments and to make two independent mass assignments. The PA and PB counters detected protons and alpha particles, since any un-interacted fragment with $Z > 2$ stopped in the second CsI crystal.

The detector was designed with two criteria in mind: to minimize the fraction of fragments which interacted in the detector, and to make two independent measurements of the mass of each fragment. The first dictated the use of heavy (CsI) crystals and SF-6 glass in order to keep the interaction length as large as possible. The second simiplified the analysis of such a large data set and provided redundancy. The two mass determinators were a particle-identifier using the delta E and E crystals and a similar one using the Cherenkov and E crystal for fragments with $Z > 2$.

The S1 counter had a single 11-stage photomultiplier tube with iris diaphragm. The CsI crystals were enclosed in small diffusion boxes and were

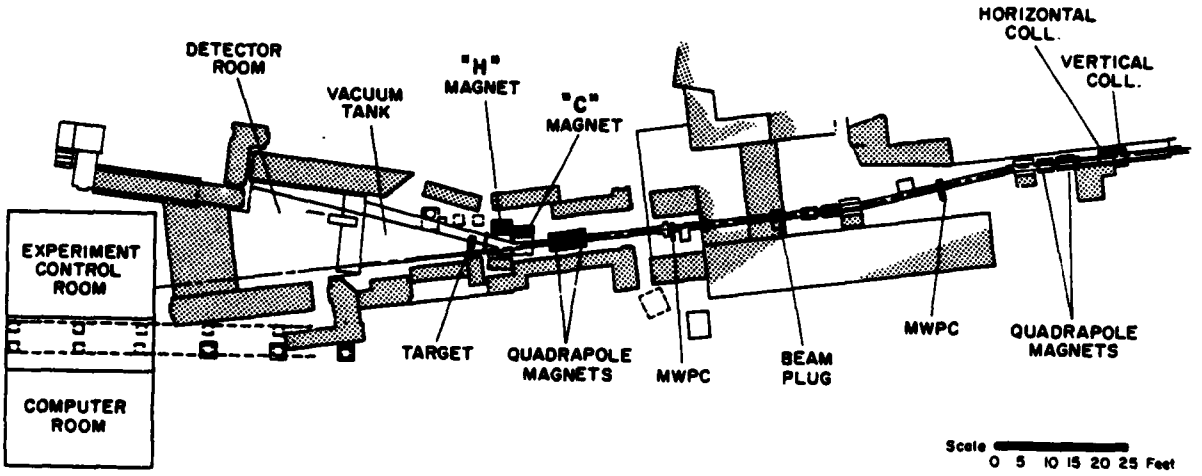

Fig. 1 — Beam line no. 40 at Lawrence Berkeley Laboratory Bevatron accelerator. The detector is in the forward end of the detector room immediately down stream from the vacuum tank.

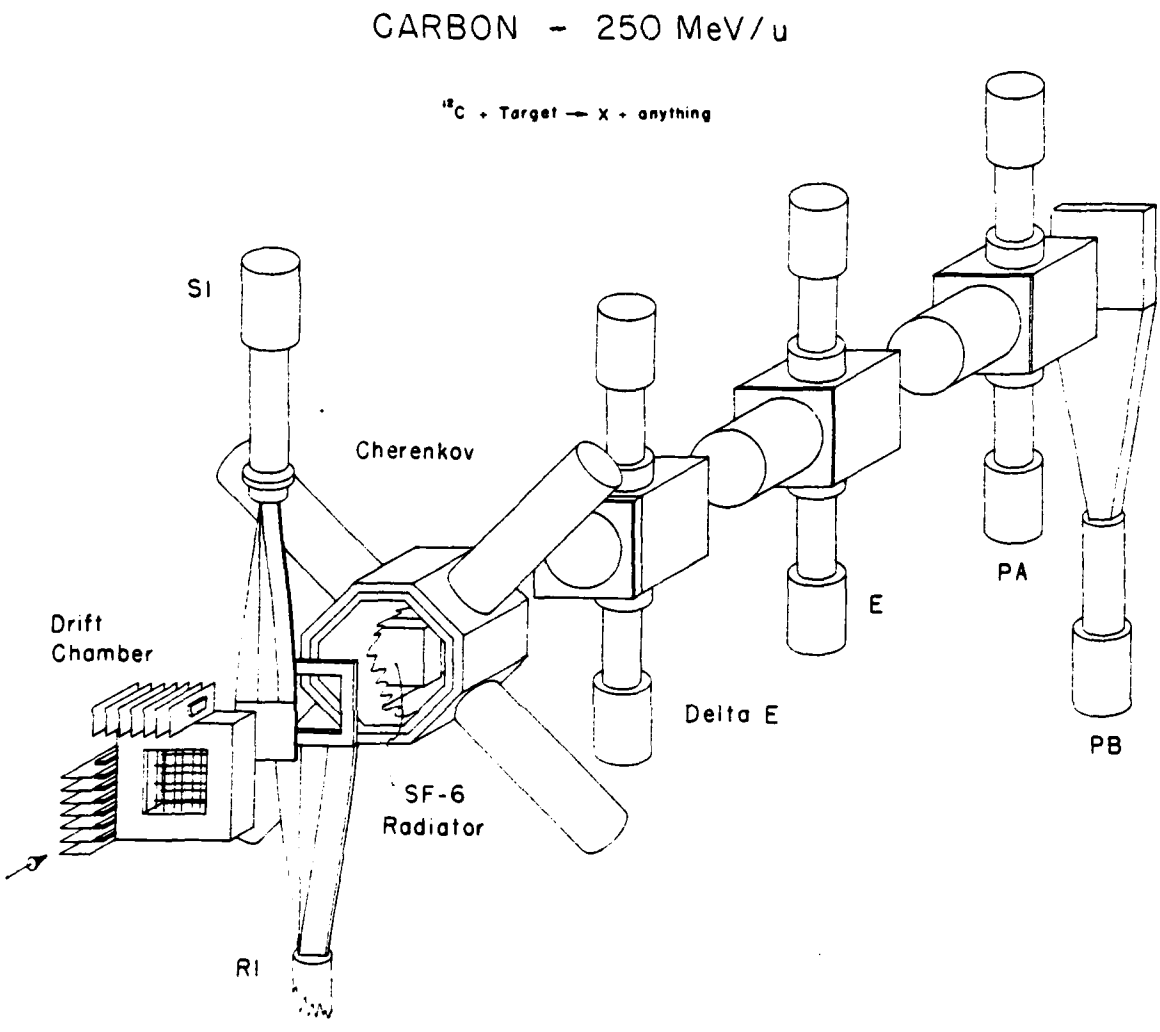

Fig. 2 — An orthographic projection of the N.R.L. heavy ion detector

Table I — The detector

ELEMENT	SIZE & MAT'L	DENSITY	RESOLUTION-MEASURED WITH 245 MeV/u ^{12}C Beam (σ/Mean)
S1	2 1/2" x 2 1/2" x 1/4" PILOT B	1.02 g/m^3	4.3%
R1	3 1/2" x 3 1/2" x 1/4" PILOT B	1.02 g/cm^3	(Logic only)
Cherenkov	2 1/2" x 2 1/2" x 7/8" SF-6 Glass	5.18 g/cm^3	7.9%
Delta E	3" CYL. x 3/8" CsI	4.51 g/cm^3	2.3%
E	3" CYL. x 3" CsI	4.51 g/cm^3	1.9%
P	3" CYL.x 3" NaI	3.67 g/cm^3	~2%
PB	3" x 3" 1/2" PILOT B	1.02 g/cm^3	(Logic Only)

each viewed by two 11-stage tubes. The Cherenkov counter diffusion box was viewed by four matched 8575 tubes. Photoelectron statistics made a negligible contribution to the resolution for all fragments, and the energy deposition distributions were quite symmetric, with the exception of those from the Cherenkov counter.

In the delta E CsI counter, the isotopes of a particular species all lost very nearly the same amount of energy in the counter. However, the mass of each isotope is different so that the total energy was distributed among a different number of nucleons. Thus, when they entered the E CsI (total energy) crystal, the amount of energy they deposited was a strong function of their mass. This technique gave excellent isotopic resolution.

The fast signals (S1, Cherenkov and PB) were put into an 11-Bit Camac A.D.C. with a 50 ns gate. The slow crystal signals were put into another 11-bit A.D.C. with a 3 μsec gate. All dynode signals were put into a redundant peak sensing A.D.C. The drift chamber signals were amplified at the front end by Lecroy TR4500 amplifiers, then discriminated and put into 11-bit T.D.C.'s in the Camac crate.

The target thickness was chosen in order to keep the multiple Coulomb scattering to ~2 mrad. This was a compromise between a reasonable amount of beam time per data file and accurate momentum measurements. The momentum distributions are so narrow that even 2 mrad could produce an uncertainty in the momentum which was a non-trivial fraction of the width (~120 MeV/c) of the momentum distribution.

3. Beam Monitor:

The beam monitor system is also shown in Figure 3. This is the standard system used on Bevalac beam Line 40. It is composed of three parts. The first part is a counter in particle mode which counts up to 5×10^4. The second part is the "current mode" which takes over above 5×10^4. This is the signal from the last dynode of the COU into a current to frequency converter. The third part is a secondary emission monitor consisting of three small counters positioned $\sim 45^{o}$ from a small foil downstream from the

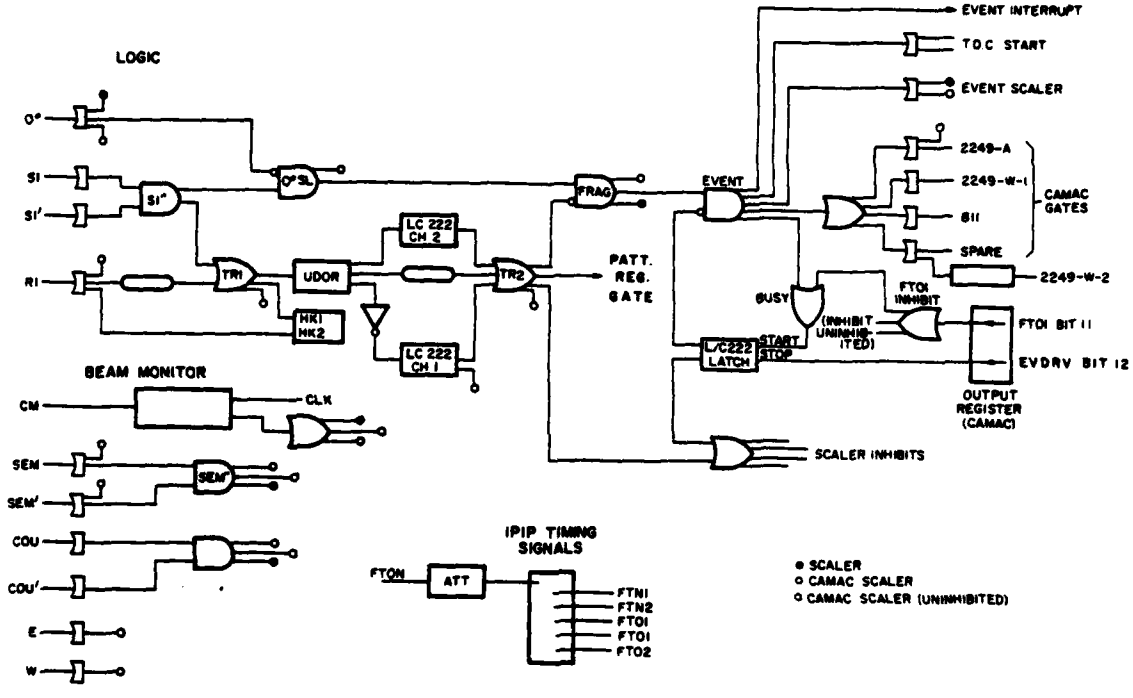

Fig. 3 — The fast logic for this experiment, as well as the beam monitor system and the IPIP timing signals

COII counters. This gives independent information at high rates. Various combinations of doubles and triples from these counters give counting rates which are 10^{-1} to 10^{-6} of the beam. The system is calibrated by bringing the beam up slowly at the beginning of each run and, off-line, doing a least squares fit of all counters and combinations to :OU. This, with their individual variances, gives beam intensity information with an uncertainty of ~1%.

4. Fast Logic:

The fast logic is shown in Figure 3. There are several points to make about this type of logic. The logic between TR1 and TR2 copes with all known bevatron beam pathology, and will not give a TR2 pulse no matter how long the pathological behavior lasts. An event trigger is defined as a combination of logic signals which indicate that the Camac crate must be read out. An S1.S1'.TR2 and a 'computer not busy' define an event trigger. This signal is used to generate an event interrupt, start the T.D.C.'s, and generate all Camac gates. Various timing signals in the acquisition code appear at an output register in the Camac crate. Among these signals, FT01 and EVDRV define computer busy as well as inhibit signals for the scaler bank in the Camac crate. Several housekeeping bits were recorded with each event. The first was recorded whenever R1 gave a signal (out of geometry), the second whenever S1 was associated with an R1 signal, and finally any signal at S1 when the A.D.C. gates were open (not shown).

The IPIP signal is the master Bevatron timing signal. This was conver' ; into timing signals which covered the entire accelerator beam spill and were used in scheduling data acquisition tasks.

5. Running System Software:

The software for an experiment of this type is by far the most complex part of the system and is divided into three parts:

1. Data Acquisition and fast analysis
2. Experiment control
3. On-line slow analysis and graphics

Figure 4 is a schematic drawing of the software system tasks. The data acquisition tasks and drivers which are active during the machine spill are SKEDUL, IMDRV, RUNDTA and EVDRV. These tasks are assisted by FTEND, FTDISP and FILEND which operate between spills or at the end of a data file. The MASTER line of tasks is to control the experiment and CREEP is the slow analysis. Because of the complexity of the system, its explanation is in Appendix A.

6. Analysis and Preliminary Results:

The analysis of the data proceeds in four steps: (1) normalization of event and scaler data, (2) definition of chi square logic and construction of physics tape code, (3) production run of all data files and (4) tabulation of final cross sections and momentum distribution widths and offsets. We are ready for the production run, and the results presented here represent less than 1%of the data.

A. Normalization:

Even though we have two mass determinations for each event, each mass identifier must be normalized. The first mass assignment uses the particle identifier technique. This may be described as the optimum way to use the information from both the stopping detector and the preceding detector (E and delta E). The range at entry to the delta E counter may be written:

$$R = K \frac{M}{Z^2} M^{-\alpha} \varepsilon^{\alpha} + T = K \frac{M}{Z^2} M^{-\alpha} (\varepsilon + \Delta\varepsilon)^{\alpha}, \text{ for } Z > 2.$$

$\Delta\varepsilon$ and ε are the kinetic energies at entry to the delta E and E counters, and T is the thickness of the delta E counter. Then

$$Z^2 M^{\alpha-1} = K' [(\varepsilon + \Delta\varepsilon)^{\alpha} - (\varepsilon)^{\alpha}]$$

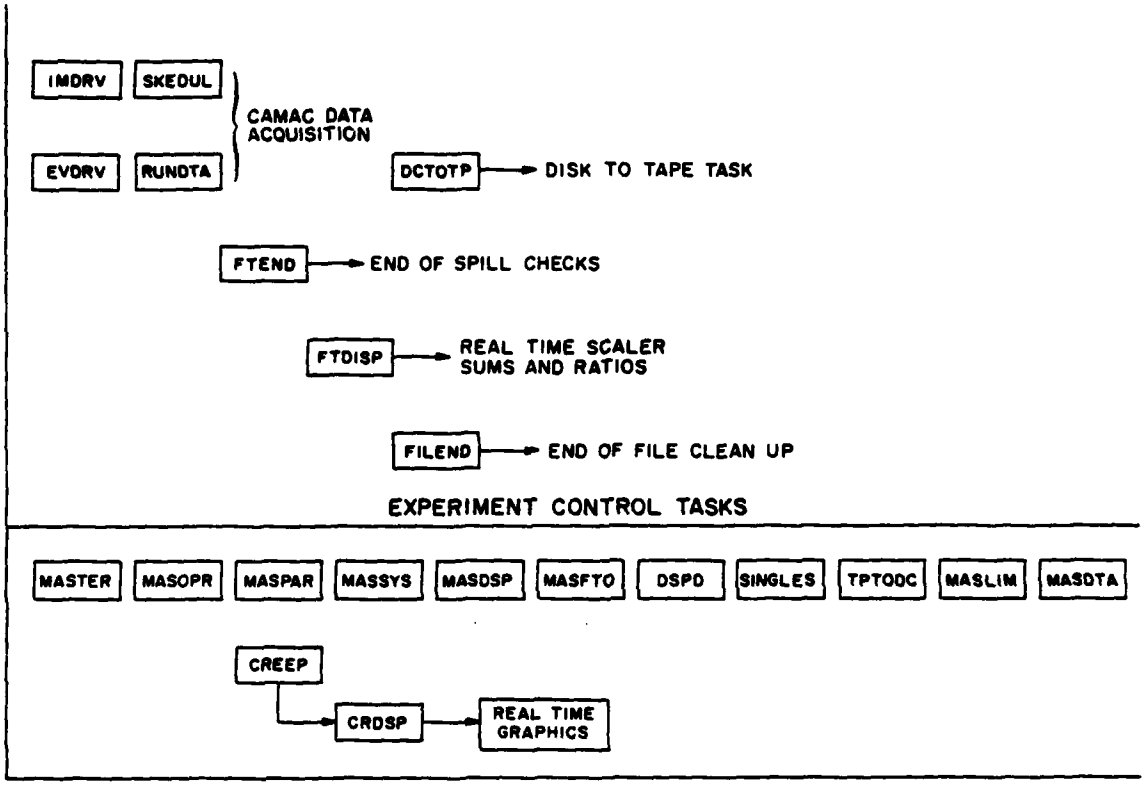

Fig. 4 — The tasks and drivers for the software running system. The vertical scale is priority.

and the particle identifier, P.I. is:

$$P.\ I. = M = \left[\frac{K'}{Z^2}\ (\varepsilon + \Delta\varepsilon)^{\alpha} - (\varepsilon)^{\alpha}\right]^{1/\alpha - 1}$$

The exponent, α, is very close to the expected 1.68 with a very weak charge dependence.

The second mass assignment for $Z > 2$ uses the Cherenkov and E counters in the spirit of the particle identifier even though they are not adjacent detectors. Nevertheless, this approach leads to a very high resolution mass determination. For a penetrating Cherenkov detector (thick radiator), the signal is an integral, over the radiator, of the Cherenkov signal ($\propto Z^2$) times the effective range ($\propto A/Z^2$) which yields a signal proportional to the mass:

$$S_C = K \int_{rad} C\ \frac{Z^2}{A}\ F(\beta)d\beta = K \int_{rad} Z^2\ f(\beta)\ \frac{M}{Z^2} F(\beta)d\beta$$

$$= M\ G(\beta),\ \text{or}$$

$$= M\ R^{\delta},\ \text{where } R \text{ is the range and } \delta \text{ is an exponent.}$$

The range is related to the stopping detector signal (E counter) by:

$$R \propto M^{-0.69} S_E$$

Then we have:

$$\frac{S_C}{M} \propto (M^{-0.69})^{\delta}\ S_E{}^{\delta}\ ,\ \text{or}$$

$$M^{\lambda} \propto \frac{S_E{}^{\delta}}{S_C}$$

The Cherenkov - E mass (C.E. mass) has considerably better resolution than the mass assignment using the particle identifier because it combines the two detectors with the most information. The two exponents, λ and δ, were found for each charge.

Both mass assignments are shown in Figure 5 for $Z > 2$. Note that for $Z > 3$ the C. E. assignment is significantly better but by $Z = 6$ the resolutions are comparable. This figure is intended to show in a qualitative way the relative resolution at the two determinators.

The helium isotopes were separated in a slightly different manner. Since the isotopes stopped in different elements of the detector, no P. I. mass determinator could be formed. However, a Cherenkov-E type of mass assignment worked well. This was helped by the fact that all ^3He stopped in the E counter, and the other isotopes did not. The protons, deuterons and tritons were not resolved, because the photoelectrons in the Cherenkov counter were too few to resolve these isotopes reliably.

The last step in the normalization is to construct the chi square of the form:

$$X^2(Z, M, \beta) = \frac{(S1 - S1')^2}{\sigma_{S1}^2} + \frac{(S_C - S_C')^2}{\sigma_C^2} + \frac{(S_{\Delta E} - S_{\Delta E}')^2}{\sigma_{\Delta E}^2} + \frac{(S_E - S_E')^2}{\sigma_E^2}$$

for $Z > 2$.

The primed quantities are data and the others are to be determined. This is a large undertaking because each term of the chi square must be determined from the data and normalized to unity for each isotope at the 1% level.

The total production cross sections are determined by integration of the eight angular measurements. The errors are primarily statistical. For the more abundant isotopes, this yields cross sections at the 1% level.

B. Momentum Distributions:

The velocity, β, and mass, A, measurements were combined to produce the momentum quantities of interest. The quantities in the laboratory system are the longitudinal, P_n, and transverse, P_t, momenta:

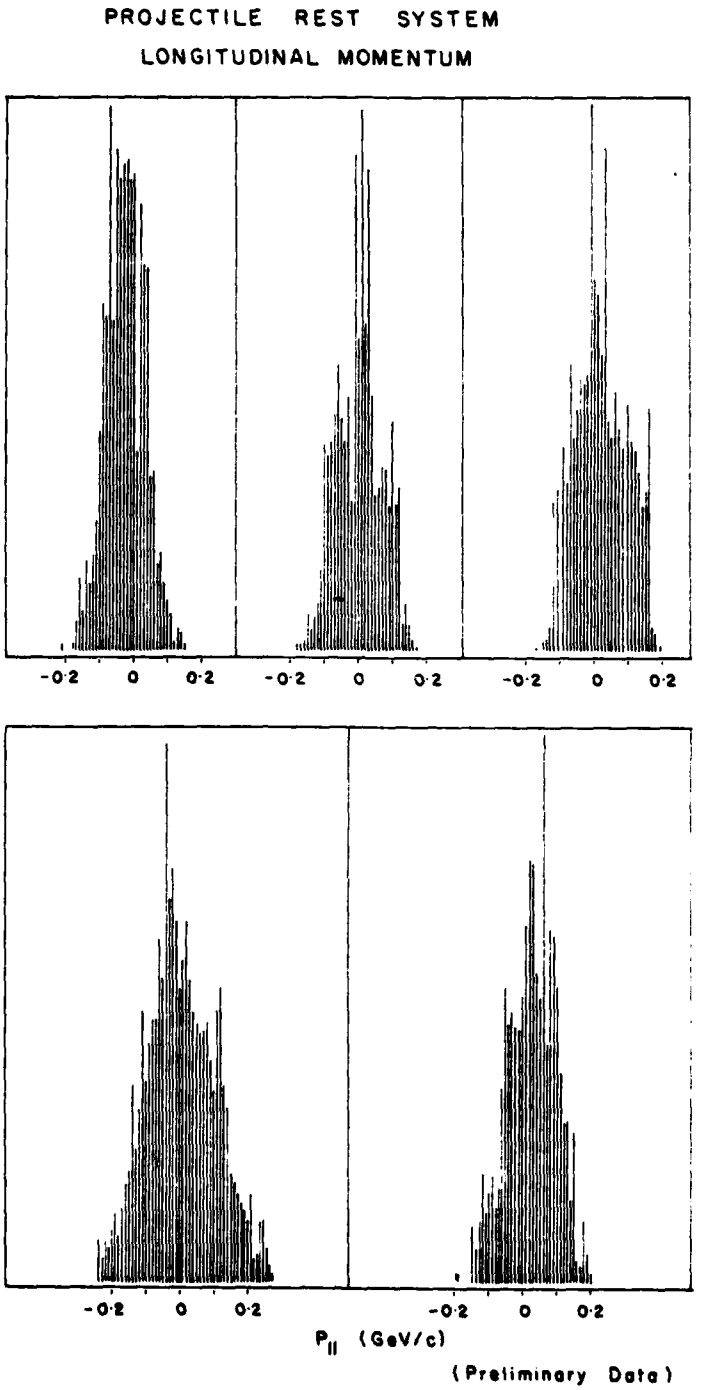

Fig. 5 — The Particle - Identifier, P.I. and the Cherenkov-E, C.E. mass determinators for $Z>2$. The number of events in each histogram varies, but is typically two to three hundred.

$P_{\parallel} = \gamma\beta\ M_0\ A\ \mathrm{Cos}(\theta)$

$P_t = \gamma\beta\ M_0\ A\ \mathrm{Sin}(\theta)$, where M_0 = 931.5 MeV.

The longitudinal momentum in the projectile rest system is:

$P_{\parallel} = \gamma_0(P - \beta_0(\gamma m_0 A))$, where γ_0 and β_0 are those of the beam.

Figure 6 shows the transverse and longitudinal laboratory momenta for a sample of 1500 events. Note that the widths of the distributions are indeed similar if not identical.

Figure 7 shows the projectile rest system momenta for selected isotopes. The isotopes from upper left are ^{4}He, ^{6}Li, ^{7}Be, ^{11}B and ^{12}C. In a qualitative way, the parabolic mass dependence of the widths of the distributions, first seen at 1.05 and 2.1 [3] GeV, is evident. That is, ^{4}He and ^{12}C are narrow and ^{7}Be is widest.

C. Chi Square Logic and Physics Tape Code:

The next step is to decide on the chi square logic for processing an entire data file. This is fairly complicated but the spirit is to examine each trigger. Only those within geometry (3 cm. radius from the center of the detector) are defined as events. The first level word list is computed for each event. If the P.I. mass and the C.E. mass agree and the chi square is less than 3.0, the rest of the word list is computed. Then each distribution of any quantity to be saved is divided into the appropriate number of bins in a large common area of 110,000 words, and for this event the appropriate bins are incremented. If the masses do not agree or the chi square is greater than three, minimization routines are called and the event is processed further. If the chi square remains large, the event is incremented into another part of the common area in order that the chi square distribution for these events may be examined for structure. This method of handling the completed word lists allows the data set to be expanded and then compressed by a factor of nearly a thousand.

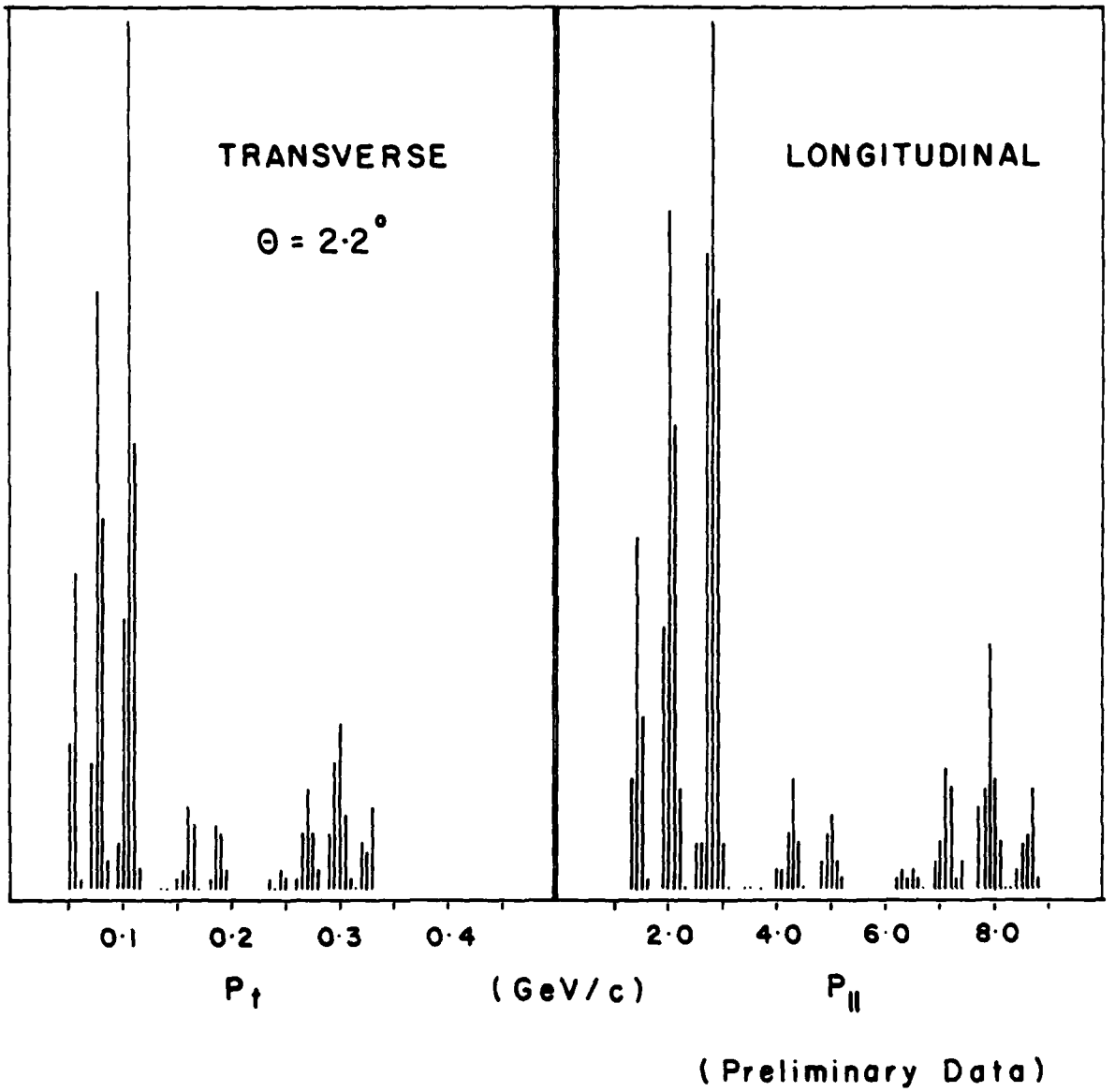

Fig. 6 — The laboratory longitudinal and transverse momentum distributions at $\theta = 2.2°$. The preliminary distributions shown here contain ~1500 events.

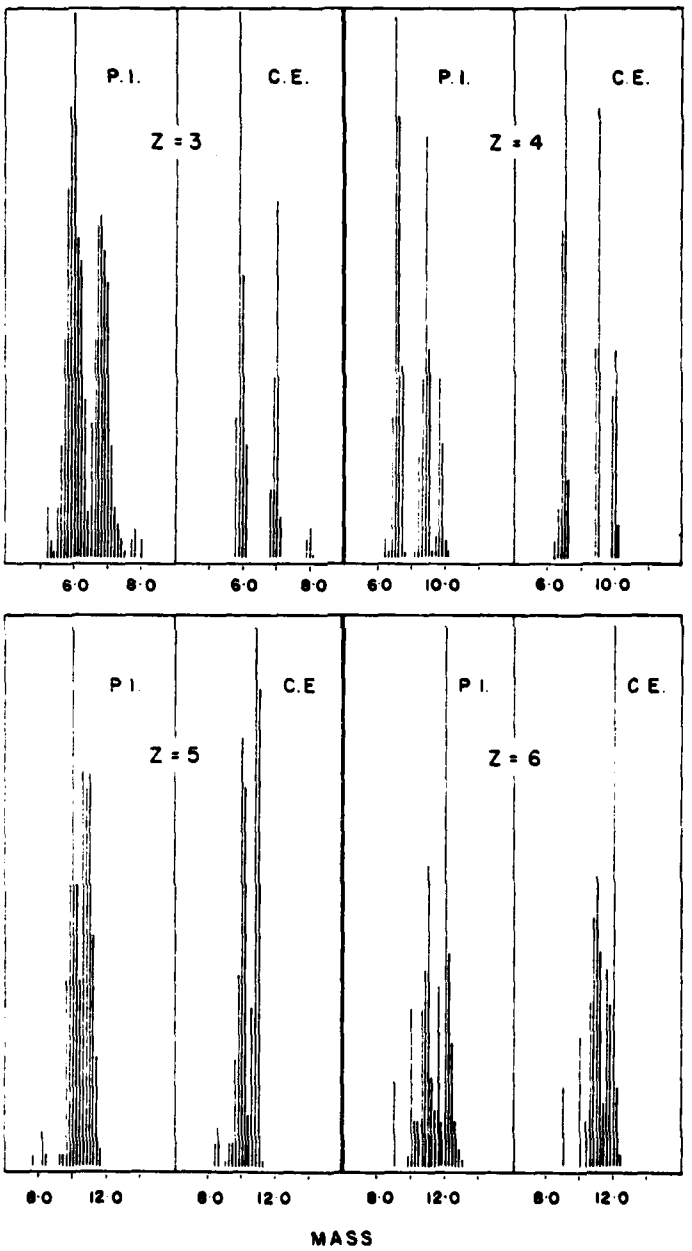

Fig. 7 — The longitudinal momentum distributions in the projectile rest system. The isotopes are ^{4}He, ^{6}Li, ^{7}Be, ^{11}B and ^{12}C. These distributions are small samples containing several hundred events each.

7. Discussion of Results:

A great deal can be learned about the fragmentation process from the energy and target dependence of the isotopic production cross sections and momentum distributions.

The cross sections factor accurately down to 1.05 GeV/u,[1]

$$\sigma_{BT}^{F} = \gamma_B^F \gamma_T,$$

where B, F, T, are the beam, fragment and target. The target factor may be fit to:

$$\gamma_T \simeq (A_B^{1/3} + A_T^{1/3} - 0.8)$$

which implies a peripheral interaction with the target. This relation holds except for light targets, and it is enhanced for the heaviest targets by single nucleon stripping. Precisely why this relation does not work for light targets is not known. The enhancement in γ_T for single nucleon stripping for high Z targets has been interpreted successfully via a giant dipole resonance in the virtual photon field of the target.[2] This enchancement should not be observed at 250 MeV/u if this interpretation is correct.

Another question this experiment addresses is the factorization of the partial cross sections and the dependence of the target factor on A_B and A_T at 250 MeV/u. Put another way, if the condition for limiting fragmentation is a large separation in rapidity, Y ($Y=\tanh^{-1}(P_{\parallel}/E)$ where $P_{\parallel}$ and E are longitudal momentum and total energy) between target and fragment, is the separation large enough at this energy?

A similar question can be asked of the momentum distributions and their possible energy and target dependence. Limiting fragmentation requires that the shape of the momentum distributions be independent of the target and projectile. This has been demonstrated nicely at 1.05 GeV/u for ^{12}C and ^{16}O.[3] The distributions of the transverse and longitudinal momentum

in the projectile rest frame are Gaussian--implying that the fragments are emitted isotropically in this frame with very small energy transfers.[3] The preliminary distributions from this experiment are indeed consistent with this behavior at this energy.

The mass dependence of the widths can be fitted, although with a large chi square, to a parabolic shape predicted by three independent theories.[4-7] The widths in this experiment exhibit the same behavior; indeed it would be surprising if the parabolic shape were not true in some approximation, as it arises from such reasonable and modest assumptions. It may be that the fit is bad because nuclear structure effects are important in determining the individual widths, as pointed out by Greiner et al.[3]

The parabolic mass dependence allows the Fermi momentum and the excitation energy to be derived. The excitation energy is, within errors, equal to the binding energy, implying little energy transfer from the target to the fragment, a reasonable and consistent conclusion at 1.05 GeV/u. This experiment exhibits similar behavior in the preliminary data.

Large transverse momentum fragments will be easily observed in this experiment. This is important because any departure from Gaussian behavior for any final state would lead to different cross section as measured by our detector and the spectrometer of Lindstrom et al.[1] which measures within 12.5 mrad about 0^{o}.

Finally, some very interesting results by Gelbke et al. indicate that the cross sections for ^{16}O projectiles on heavy targets are very similar at 20 MeV/u and 2.1 GeV/u. On the other hand, a comparison of the 20 MeV/u data with that at 9 MeV/u shows that the cross sections differ markedly. These authors point out that this behavior may corroborate the suggestion[9] that the relative partial cross sections may vary significantly for relative velocities; smaller than the Fermi velocity and constant for larger velocities. They could not determine the dependence of γ_T on A_B at 20 MeV/u.[8]

An experiment of this type which supplies complete and accurate information at intermediate energy is essential to the resolution of these questions.

8. APPENDIX A:

Readout and Fast On-Line Analysis:

This part of the system is designed around the spill structure of the Bevatron which is a one second spill every four seconds. The FTO1 signal shown in Figure 3 is the highest priority interrupt. It allows SKEDUL (Figure 4) to install RUNDTA, because this task is too large to remain in core except during the spill. RUNDTA enables the event interrupt register in the Camac crate and starts reading events at FTN2. Until a QIQ is completed or a core buffer is filled, the CRAWL routines in RUNDTA, perform checks on the data asynchronously with the readout while the data is still in the core buffer (fast analysis). Any errors are written to global common to be picked up by FTEND. The buffers are written to disk by RUNDTA as they are filled. At the end of the spill, RUNDTA reads the scaler bank, disables the event interrupt register, schedules the task FTEND and exits.

The task FTEND does the first level of checks on the experiment itself, i.e., the target and beam and detector positions. If it finds any malfunction or error condition, it lights one of 16 L.E.D.'s in an I/O register in the Camac crate to warn the operator. It then records the condition in the computerized log book, and if the error is serious it stops data taking. It then stores the disk and core pointers for RUNDTA. Finally it checks for a full disk. If the disk is full, FILEND is called, otherwise the flat top over displays are called.

The task FTDISP displays the results of the fast analysis in various formats as well as the scaler data from the last spill and the sums from the beginning of the run.

Experiment Control:

The list of tasks starting with MASTER in Figure 4 are the experiment control tasks. MASTER is the dispatcher task for all of the control tasks, because the tasks are disk resident unless they are active.

MASOPR is the main experimental control task. The options for end of data file and tape control are selected here as well as those for starting and stopping data taking.

MASPAR is the detector and target control task, and contains the hardcopy options at the end of a data file.

FTODSP is the task which calls the selected flat top over display option.

MASSYS allows the reassignment of Logical Unit Numbers to all I/O devices, and is the control task for the fast and slow analysts. It also contains the global common debugging routines.

MASDSP allows the selection of the display option (number of histograms and scatter plots) and the specification of cuts and limits for the slow analysis.

MASFTO is the control task for the flat top over displays.

DSPD is the task which controls the VT-11 Graphics terminal . It is called by CREEP when the slow analysis display buffer is full.

SINGLES is a collection of tasks which allow each channel of each station number in the Camac crate to be read out in a lam-driven mode, to the CRT or the VT-11. It allows the 352 channels in the crate to be checked and calibrated individually or in concert.

MASLIM allows limits to be written to global common which are used by FTEND and FILEND.

MASDTA allows constants, conversion factors and exponents to be written to global common for use by CREEP in the higher analysis levels. This is necessary for taking calibrated data.

Slow On-Line Analysis:

The lowest priority task is CREEP. This task brings a buffer of data in from the disk, and computes a word list for each event (a list of words derived from the raw data). The length of the list is optional and varies from raw data to a full list including mass and velocity assignments. Any group of words from this list may be selected for display on the VT-11. A maximum of four histograms or four scatter plots can be displayed simultaneously. The limits and cuts can be changed and the same data replotted. The analysis is slow in the sense that the displays appear up to a minute after the data has been taken. This depends on the data rate and therefore how much computer time was available to CREEP.

9. ACKNOWLEDGEMENTS:

The number of people who helped design, construct, stage, run and analyze this experiment is large. We thank L. Beahm for her indispensible efforts in putting together the real-time running system and debugging it at the Bevatron. We are indebted to B. Stiller for calibrating all phototubes and for his help in assembly and calibration of the detector elements. G. Mueller was invaluable for his help, at any time, in software development. We are especially indebted to all of what is now the H.I.S.S. - A group at L. B. L. In particular, to P. J. Lindstrom, C. McParland and H. J. Crawford. We thank the entire group for lending a collective hand for our final data taking. We also thank P. J. Lindstrom for his tireless and tenacious efforts to help perfect the analysis code.

10. REFERENCES

1. Lindstrom, P.J., Greiner, D.E., Heckman, H.H., Cork, B., and Bieser, F. S., Lawrence Berkeley Lab. Preprint, LBL-3650 (1975).
2. Heckman, H.H., and Linstrom, P.J., Preprint, LBL-4380 (1976).
3. Greiner, D.E., Lindstrom, P.J., Heckman, H.H., Cork, B., and Bieser, F.S., Phys. Rev. Lett. 35, 152 (1975).
4. Wenzel, W.A., Proc. L.B.L. Heavy-Ion Seminar (unpublished).
5. Lepore, J.V., and Riddell, R.J., L.B.L. 3086 (1974).
6. Feshbaca, H. and Huang, K., Phys. Lett. 47B, 300 (1973).
7. Goldhaber, A.S., Phys. Lett. 53B, 306 (1974).
8. Gelbke, C.K., Buenard, M., Hendrie, D.L., Mahoney, J., Mermaz, M.C., Olmev, C. and Scott, D.K., Phys. Lett. 65-B, 227 (1976).
9. Buenerd, H., et al., LBL-5067 (1976).
10. Shapiro, M.M. and Silberberg, R., Ann. Rev. Nucl. Sci. 20 (1970) and Phil. Trans. R. Soc. Lond. A 277, 317 (1974).
11. Wefel, J.P., Kidd, J.M., Vosburgh, K.G., and Schimmerling, W., 13th International Cosmis Ray Conference, 1, 540, (1973).
12. Kidd, J.M., Wefel, J.P., Schimmerling, W., Vosburgh, K., 14th International Cosmic Ray Conference, 2, 510, (1975).
13. Cumming, J.B., Haustein, P.E., Stoener, R.W., Mausner, L., and Naumann, R.A., Phys. Rev. C, 10, 739 (1974).
14. Skoski, L., Merker, M. and Shen, B.S.P., Phys. Rev. Lett. 30, 51, (1973).
15. Heckman, H.H., Greiner, D.E., Lindstrom, P.J., and Bieser, F.S., Phys. Rev. Lett., 28, 926, (1972).
16. Lindstrom, P.J., Greiner, D.E., Heckman, H.H., Cork, B., Bieser, F.S., 14th International Cosmic Ray Conference, 7, 2315, (1975).
17. Raisbeck, G.M. and Yiou, F., 14th International Cosmic Ray Conf., Munich, 2, 502 (1975).
18. Raisbeck, G.M., and Lestringuez, J., and Yiou, F., 14th International Cosmic Ray Conf., Munich, 2, 499 (1975).
19. Wefel, J., Kidd, J., Vosburgh, K. and Schimmerling, W., Phys. Rev. C. 19, No. 4, 1380, (1979).
20. Jakobsson, B., Kullberg, R. and Otterlund, I., C. R. Phys. Report LUIP-CR-75-02 (1975).

21. Raisbeck, G.M. and Yiou, F., Phys. Rev. Lett. 35, 155 (1975).
22. Silberberg, R., and Tsao, C.H., Ap. J. Suppl., 25. 315 (1973).
23. Fontes, P., Perron, C., Lestringuez, J., Yiou, F., and Bernas, R., Nucl. Phys. A165, 405 (1971).
24. Yiou, F., Raisbeck, G., Perron, C. and Fontes, P., 13th International Cosmic Ray Conf., 1, 512 (1973).
25. Poskanzer, A.M., Sextro, R.G., Zebelman, A.M., Gutbrod, H.H., Sandoval, A., and Stock, R. Phys. Rev. Lett. 35, 1701 (1975).
26. Scott, D.K., Private communication.
27. Westfall, G. D., et al., Phys. Rev. Lett. 43. 1859, (1979).9.


FILMED
8